Conus medullaris teratoma in an adult: A case report and literature review

TING REN[1], LINFENG SONG[1], XU CHEN[1], HANG ZHANG[1], YIYUN ZHANG[1], LUNYOU ZHANG[2] and LIN JIANG[1]

[1]Department of Radiology, The Third Affiliated Hospital of Zunyi Medical University (The First People's Hospital of Zunyi), Zunyi, Guizhou 563000, P.R. China; [2]Department of Pathology, The Third Affiliated Hospital of Zunyi Medical University (The First People's Hospital of Zunyi), Zunyi, Guizhou 563000, P.R. China

Received April 21, 2026; Accepted October 6, 2026

DOI: 10.3892/etm.2026.13353

Abstract. Spinal teratomas arise from embryonic germ cells. The present case report describes a 54-year-old male patient with recurrent low back pain accompanied by radiating pain and numbness in the left lower limb for >1 month. CT and MRI revealed an irregular lesion in the conus medullaris. Gross total resection was achieved, with histopathological examination determining an intramedullary mature teratoma (IMMT). No new postoperative neurological deficits occurred. At the final outpatient follow-up, ~4 months after surgery, the lower back pain and radiating pain had markedly improved, although mild numbness persisted in the left lower limb. Adult conus medullaris IMMTs are rare and prone to preoperative misdiagnosis due to their unusual location and heterogeneous imaging appearance. To improve recognition of these tumors, the present report describes the clinical, imaging and pathological features of the present case and briefly reviews similar cases. The combined presence of calcification, focal fat, cystic components and heterogeneous enhancement may prompt the consideration of IMMT in the differential diagnosis of conus medullaris lesions and reduce the risk of diagnostic error.

Introduction

Spinal teratomas are rare primary spinal tumors consisting of tissues derived from multiple embryonic germ layers and account for 0.1-0.5% of all spinal cord tumors. Intramedullary mature teratomas (IMMTs) are particularly uncommon in adults, with a previous literature review having identified only 57 adult cases reported (1). The pathogenesis of spinal teratomas remains uncertain, although the aberrant migration or persistence of pluripotent embryonic cells during early development has been proposed (2). Given their presumed developmental origin, current management focuses on early recognition and appropriate treatment rather than primary prevention. Such tumors most frequently occur in the lumbosacral region (3). Diagnosis may be challenging as clinical manifestations are non-specific and imaging appearances vary with tumor composition. CT scans are useful in identifying calcified or ossified components, whereas MRI better characterizes fatty, cystic and soft-tissue components; yet definitive diagnosis relies on histopathological examination (4,5). Surgical resection is the primary treatment for symptomatic spinal teratomas. Gross total resection is preferred when safely achievable, whereas subtotal resection may be necessary when the lesion is tightly adherent to the spinal cord, conus medullaris or adjacent neural structures. Long-term postoperative surveillance is recommended, particularly after incomplete resection (6-8). The present report describes a 54-year-old male patient with a conus medullaris lesion that was initially considered to be a myxopapillary ependymoma but was subsequently diagnosed as an intramedullary mature teratoma (IMMT), following surgical resection and histopathological examination. These lesions may mimic more common intramedullary tumors upon imaging, particularly myxopapillary ependymoma (4). By compiling the CT, MRI, histopathological and immunohistochemical findings with a brief review of previously reported similar cases, the present report highlights imaging features, including calcification, focal fat, cystic components and heterogeneous enhancement, that may improve preoperative recognition and reduce the risk of diagnostic error (4,9).

Case report

A 54-year-old male patient presented to the Department of Orthopedics within the Spine Surgery Clinic of The Third Affiliated Hospital of Zunyi Medical University (The First People's Hospital of Zunyi; Zunyi, China) in May 2025, with recurrent low back pain accompanied by radiating pain and numbness in the left lower limb for >1 month, without an identifiable precipitating event. Lumbar CT and thoracolumbar MRI were performed on days 1 and 2 of patient presentation to

Correspondence to: Professor Lin Jiang, Department of Radiology, The Third Affiliated Hospital of Zunyi Medical University (The First People's Hospital of Zunyi), 98 Fenghuangbei Street, Zunyi, Guizhou 563000, P.R. China
E-mail: jlinzmc@163.com

Key words: intramedullary mature teratoma, spinal cord tumor, adults, MRI, CT

the Department of Orthopedics. The patient was subsequently evaluated at the Neurosurgery Outpatient Clinic at The Third Affiliated Hospital of Zunyi Medical University (The First People's Hospital of Zunyi; Zunyi, China) 3 days later and was admitted to the Department of Neurosurgery of The Third Affiliated Hospital of Zunyi Medical University (The First People's Hospital of Zunyi; Zunyi, China) 9 days after the initial outpatient visit, for further evaluation and surgical management. Laboratory tests, including complete blood count, urinalysis, liver and renal function tests, serum electrolytes, blood glucose and glycated hemoglobin, coagulation testing and hepatitis B serology, were conducted. Preoperative testing showed elevated aspartate aminotransferase and alanine aminotransferase levels (both, 68 U/l; reference range, 10-40 U/l), blood glucose (10.8 mmol/l; reference range, 3.9-6.1 mmol/l) and glycated hemoglobin (6.7%; reference range, 4.1-6.2%). The remaining hematological, biochemical, urinalysis and coagulation results fell within their respective normal reference ranges. Physical examination revealed flattening of the lumbar lordosis, paraspinal muscle spasm and restricted lumbar mobility. Hypoesthesia was present over the lateral aspect of the left calf, whereas muscle strength of the left tibialis anterior and extensor hallucis longus was grade 4/5, as assessed by manual muscle testing using the 0-5 Medical Research Council scale (10). No gait disturbance, saddle anesthesia or sphincter dysfunction was identified. Fig. 1A shows the band-like calcified component at the L1 level on sagittal CT scans and Fig. 1B and C show the same calcified component on axial and coronal CT scans, respectively. No definite macroscopic fat attenuation was identified. MRI revealed an irregular lesion in the conus medullaris measuring 2.3x1.2 cm on sagittal images, with indistinct margins. On T1-weighted images (Fig. 2A and B), the lesion was predominantly hypointense with focal arcuate hyperintensity. T2-weighted images (Fig. 2C and D) demonstrated multiple small hyperintense cystic areas and linear hypointense components. On sagittal fat-suppressed T2-weighted images (Fig. 2E and F), the focal arcuate T1-hyperintense component demonstrated corresponding signal suppression, whereas the small cystic areas remained hyperintense. The linear hypointense components (Fig. 2D and F) were considered to correspond to the calcified component identified on CT. Contrast-enhanced T1-weighted images (Fig. 2G and H) demonstrated heterogeneous enhancement with small patchy non-enhancing areas. No evidence of spinal cord tethering or spina bifida was observed.

Based on the conus medullaris location, lower-limb radicular symptoms and heterogeneous enhancement, myxopapillary ependymoma was considered the leading preoperative diagnosis. However, a number of imaging findings were atypical for myxopapillary ependymoma. In particular, the band-like calcification observed on CT, with corresponding linear hypointensity on T2-weighted and fat-suppressed T2-weighted images, focal T1 hyperintensity with signal suppression on fat-suppressed T2-weighted images and multiple small hyperintense cystic areas were retrospectively considered more suggestive of a mature teratoma.

Ceftriaxone sodium (1 g) was prescribed for antimicrobial prophylaxis as a single intravenous infusion to be administered 30 min before surgery. In June 2025, 4 days after admission to the Department of Neurosurgery, the patient underwent neuronavigation-guided resection of the L1 intraspinal mass through a posterior midline approach, followed by dural repair. Gross total resection was achieved and no new postoperative neurological deficits were observed. The patient reported marked improvement in lower back pain and left lower-limb radiating pain during postoperative clinical assessment. Postoperative care included oral mecobalamin (0.5 mg three times daily) for lower-limb numbness. For postoperative analgesia, butorphanol tartrate (8 mg mixed with 50 ml 0.9% sodium chloride) was prescribed through an intravenous infusion pump at 4 ml/h. Routine monitoring and wound care were also provided. The patient was discharged 13 days after surgery.

Histopathological examination demonstrated an IMMT arising in the conus medullaris. During surgical resection in June 2025, tissue specimens were obtained from the lesion at the L1 level. Grossly, the specimen consisted of gray-white tissue fragments measuring ~2 cm in aggregate, with focal firm areas. The tissue was fixed in 10% neutral buffered formalin for 12 h at room temperature and paraffin-embedded. For H&E staining, 4-μm sections were baked at 70˚C for 1 h, deparaffinized in xylene, rehydrated through graded alcohols, stained with hematoxylin for 5 min and eosin for 1 min at room temperature, then dehydrated, cleared in xylene and mounted with neutral resin. Sections were examined using a DM750 light microscope manufactured by Leica Microsystems.

Immunohistochemistry was performed manually on 2-μm formalin-fixed, paraffin-embedded sections according to the manufacturer's instructions. After baking at 70˚C for 1 h, sections were deparaffinized and rehydrated. Antigen retrieval was performed under high pressure at 100˚C using EDTA buffer (pH 9.0) or citrate buffer (pH 6.0), as appropriate for the primary antibody, for 2.5 min, followed by standing for 5 min. Endogenous peroxidase activity was blocked with 3% hydrogen peroxide for 10 min at room temperature; no additional serum or protein blocking was performed. After PBS washing for 1 min, sections were incubated with ready-to-use primary antibodies (100 μl/section) at 37˚C for 1 h: Ki-67 (cat. no. AM0241), pan-cytokeratin (cat. no. AM0087), S100 (cat. no. AR0210), vimentin (cat. no. AM0234) and GFAP (cat. no. AM0123; all, Xiamen Talent Biomedical Technology Co., Ltd.). All primary antibodies were used as supplied at the manufacturer's ready-to-use concentrations, without further dilution. After PBS washing, sections were incubated with a ready-to-use HRP-conjugated secondary antibody (cat. no. DD13; Xiamen Talent Biomedical Technology Co., Ltd.) at 37˚C for 30 min. The ready-to-use HRP-conjugated secondary antibody was used as supplied, without further dilution. DAB (cat. no. KS-005A/B; Xiamen Talent Biomedical Technology Co., Ltd.) was applied for 5 min at room temperature, followed by hematoxylin counterstaining for 1 min at room temperature, differentiation in 1% hydrochloric acid in 75% ethanol for 1-3 secs and bluing under running water for 5 min. Sections were then dehydrated, cleared in xylene, mounted and examined using a DM750 light microscope manufactured by Leica Microsystems. H&E staining demonstrated a mature stratified squamous epithelium, with mature bone tissue, mature adipose tissue and peripheral nerve bundles observed (Fig. 3A-D). Immunohistochemical analysis demonstrated positive staining for pan-cytokeratin, S100 and vimentin,

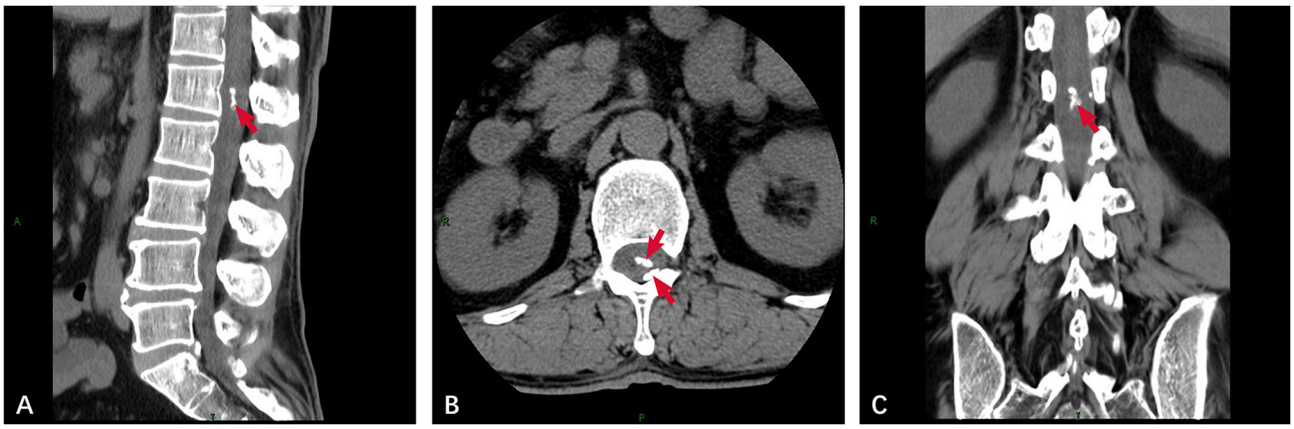


Figure 1. Preoperative CT findings. (A) Sagittal, (B) axial and (C) coronal CT images demonstrate a mixed-density lesion within the spinal canal at the L1 level. Red arrows indicate the band-like calcified component.



Figure 2. Preoperative MRI findings. (A) Sagittal T1-weighted image showing focal arcuate hyperintensity; the curved red arrow indicates the fat-containing component. (B) Sagittal T1-weighted image showing the same lesion at a different slice position; the curved red arrow indicates the T1-hyperintense fat-containing component. (C) Sagittal T2-weighted image showing numerous small hyperintense cystic areas; the red arrowhead indicates a representative cystic component. (D) Sagittal T2-weighted image shows a linear hypointense component corresponding to the calcification on CT, indicated by the red arrow. (E) Sagittal fat-suppressed T2-weighted image showing suppression of the focal T1-hyperintense component; the curved red arrow indicates the fat-containing component and the red arrowhead indicates a representative cystic component. (F) Sagittal fat-suppressed T2-weighted image showing a linear hypointense component corresponding to the calcification on CT, indicated by the red arrow. (G) Contrast-enhanced sagittal T1-weighted image showing heterogeneous enhancement of the solid component with small non-enhancing areas; the notched red arrow indicates the enhancing component. (H) Contrast-enhanced sagittal T1-weighted image showing the same lesion at a different slice position; the notched red arrow indicates the enhancing solid component.

whereas GFAP staining was negative (Fig. 4A-D). The Ki-67 proliferation index was visually estimated to be ~5% (Fig. 4E). The presence of mature epithelial, adipose, osseous and neural tissue components, together with the immunohistochemical findings, supported the diagnosis of IMMT.

The patient underwent monthly telephone follow-ups after discharge and was also assessed at outpatient visits during this period. The final available follow-up was an outpatient visit in October 2025, ~4 months after surgery. At that time, muscle strength was recorded to be 5/5 in both lower limbs, the lower back pain and radiating pain had markedly improved and only mild residual numbness persisted in the left lower limb. No additional telephone or outpatient follow-up was performed after October 2025.

Discussion

Spinal teratomas are exceedingly rare primary spinal tumors, accounting for 0.1-0.5% of all spinal cord tumors (1,2). The germ cell heterotopia hypothesis proposes that spinal teratomas arise from pluripotent embryonic cells that aberrantly migrate or become ectopically retained along the dorsal

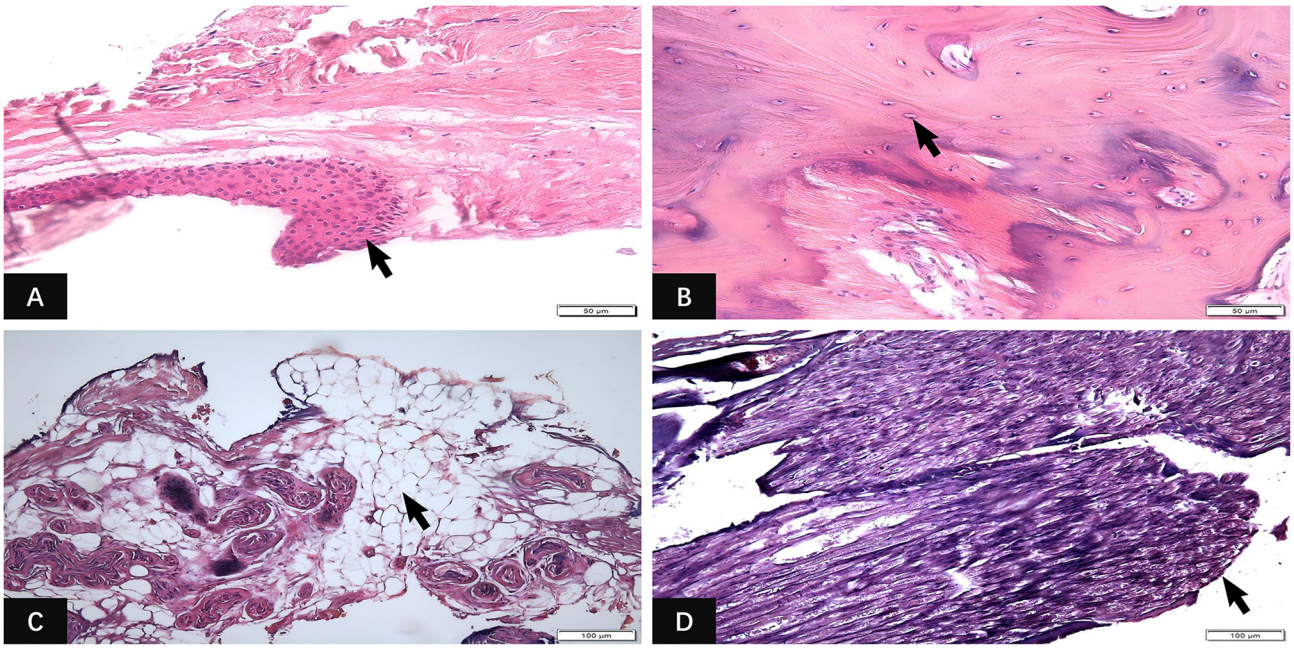


Figure 3. Histopathological findings. H&E staining demonstrates (A) mature stratified squamous epithelium, (B) mature bone tissue, (C) mature adipose tissue and (D) peripheral nerve bundles. Black arrows indicate the corresponding tissue components. Scale bars, 50 μm (A and B) and 100 μm (C and D).

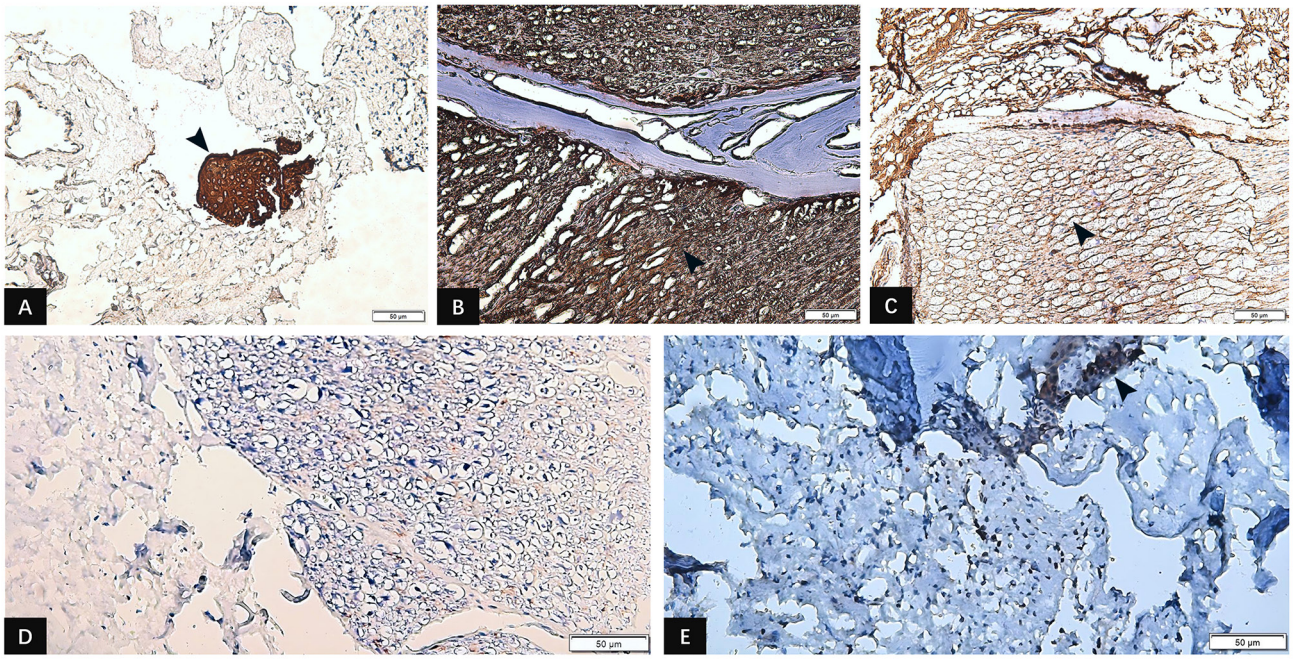


Figure 4. Immunohistochemical findings. (A) Pan-cytokeratin, (B) S100 and (C) vimentin demonstrate positive immunoreactivity, whereas (D) GFAP appears negative. (E) Representative Ki-67 immunostaining demonstrates scattered positive nuclei, with a proliferation index of ~5%. Black arrowheads in (A-C) indicate representative areas of positive brown chromogenic staining, whereas the black arrowhead in (E) indicates representative Ki-67-positive nuclei. Scale bars, 50 μm. GFAP, glial fibrillary acidic protein.

midline during early development and subsequently differentiate into tissues derived from multiple germ layers (2,3). In the present case, the presence of mature stratified squamous epithelium, bone, adipose tissue and peripheral nerve bundles appeared consistent with this hypothesis. The conus medullaris is the most common site of spinal teratomas, followed by the lower thoracic, cervical, cervicothoracic and mid-thoracic regions (1). Clinical manifestations vary according to the anatomical level of the lesion. Tumors involving the conus medullaris commonly present with low back pain, lower-limb sensory disturbances, motor weakness or sphincter dysfunction, whereas more rostral lesions may produce upper-limb weakness or quadriparesis (7,11). Associated spinal dysraphism, including spina bifida or split cord malformation, may further raise suspicion of a spinal teratoma (1,3,11). Given their rarity and heterogeneous clinical and imaging manifestations,

Table I. Previously reported adult conus medullaris and conus-adjacent spinal teratomas.

First author, year	Age, years	Sex	Tumor location	Imaging findings	Treatment strategy	Pathological subtype	Recurrence status	Follow-up duration	(Refs.)
Nonomura *et al*, 2002	33	F	T12-L1; conus medullaris	Heterogeneous T12-L1 mass; interpedicular widening, left pedicle erosion and L5 spina bifida	T12-L1 reconstructive laminoplasty; STR	Mature teratoma with ectodermal and mesodermal elements	No recurrence on MRI	8 years	(12)
Yu *et al*, 2012	34	M	L1-L2; conus medullaris; associated AVM	Heterogeneous expansile lesion; T1-FLAIR hyperintensity, mixed T2 signal and no tumor enhancement; AVM flow voids and enhancement	L1-L2 and partial T12 decompressive laminectomy; STR	Mature cystic teratoma associated with AVM	NR	2 months	(11)
Turan *et al*, 2016	48	M	L2-L3; conus medullaris	A 15x13 mm cystic lesion with a 6-mm enhancing nodule; interval enlargement and new patchy enhancement	L1-L2 decompressive laminectomies; GTR	Benign mature cystic teratoma	No residual or recurrent tumor on MRI	9 months	(8)
Mohammadi *et al*, 2017	18	M	L2-L3; intra-medullary lesion adherent to conus	A 25x22x15 mm lesion with solid and fatty components; strong enhancement of the solid component	L2-L3 laminectomy; ~90% resection (STR)	Mature teratoma; no immature or malignant elements	NR	NR	(2)
Schmidt *et al*, 2017	49	M	T12-L3; intradural lesion extending from conus medullaris	Heterogeneous T1 signal with small T2-hyperintense cystic areas; no marked enhancement	T12-L3 laminectomy; STR	Mature teratoma; no immature elements	Stable residual lesion on MRI; no progression	2 years	(16)
Kawai *et al*, 2018	23	M	T11-T12; conus-adjacent lesion with suspected intramedullary extension	A 45-mm cystic lesion with heterogeneous T2 signal, an enhancing nodule and diffuse cauda equina enhancement; no calcification on CT	T11-T12 laminectomy; STR	Mature teratoma	Regrowth and CNS-dissemination at 3 months; marked response to chemoradio-therapy	1 year	(6)
Saridakis *et al*, 2020	36	M	Medulla oblongata-L2; holocord/ panmedullary intramedullary lesion	Holocord lipoma-like lesion with T1/T2 hyperintensity and peripheral enhancement; spinal canal expansion, most pronounced at L1-L2	T9-L2 laminectomy; STR	Mature tridermal teratoma; no atypia or anaplasia	No radiological progression at 8 months; residual tumor remained	>2 years	(7)

Table I. Continued.

First author, year	Age, years	Sex	Tumor location	Imaging findings	Treatment strategy	Pathological subtype	Recurrence status	Follow-up duration	(Refs.)
Cunningham *et al*, 2022	78	F	Distal conus, L1-L4; extension into cauda equina	An 81x30x25 mm heterogeneous multicystic lesion; minimal T1 hyperintensity; conus and nerve-root compression	L1-L4 laminectomy; lesion largely removed	Mature teratoma with tissues from all three germ layers; no immature elements	NR	NR	(13)
Arora *et al*, 2022	46	M	Conus medullaris	Elongated multiloculated lesion; cauda equina root splaying; cranial fat signal; caudal T2 hypointensity and intense enhancement	Radical surgical resection	Teratoma (subtype NR)	NR	NR	(14)
Eslami *et al*, 2023	40	M	T11-L1; conus medullaris; intradural extramedullary	Large capsular lesion at T11-L1 causing spinal cord compression	T11-L1 bilateral partial laminectomy; GTR	Mature teratoma	NR	NR	(15)
Zavala-Romero *et al*, 2024	29	M	L1-L4; intradural lesion with intramedullary extension	Well-defined heterogeneous lesion; ventral T1-hyperintense fat-containing component and dorsal hypointense component; no contrast study	Bilateral L2-L4 laminotomy, microsurgical resection and laminoplasty; GTR	Mature teratoma; no immature elements	No residual tumor postoperatively; recurrence NR	5 years	(4)
Present case	54	M	L1; conus medullaris	CT: Band-like calcification; MRI: Focal fat signal, multiple small cystic areas, linear T2 hypointensity and heterogeneous enhancement	Posterior L1 resection with dural repair; GTR	Intramedullary mature teratoma	Not assessable owing to short follow-up	4 months	-

AVM, arteriovenous malformation; CNS, central nervous system; F, female; FLAIR, fluid-attenuated inversion recovery; GTR, gross total resection; M, male; NR, not reported; STR, subtotal resection.

the present case was compared with previously reported adult cases of conus medullaris and conus-adjacent spinal teratomas. Cases were eligible for inclusion if: i) The patient was an adult (≥18 years); and ii) the spinal teratoma involved the conus medullaris or an adjacent spinal level. The included cases were compared in terms of patient age, sex, tumor location, imaging findings, treatment strategy, pathological subtype, recurrence status and follow-up duration (Table I) (2,4,6,8,11-16).

Previously reported adult cases of conus medullaris and conus-adjacent spinal teratomas included patients of both sexes ranging in age from 18-78 years. The majority of patients presented with non-specific symptoms, including low back pain, lower-limb sensory disturbances, motor weakness, gait impairment and sphincter dysfunction (1,8). Radiologically, these lesions were generally heterogeneous. The coexistence of fat, cystic components, calcification, mixed signal intensities on T1- and T2-weighted images and heterogeneous or nodular enhancement may provide useful diagnostic clues for the diagnosis of mature teratoma (2,8,14). Surgical resection remains the primary treatment; however, subtotal resection may be necessary when the lesion is tightly adherent to the conus medullaris, cauda equina or adjacent neural structures. Despite mature teratomas generally having a favorable clinical course, the limited and variable follow-up periods reported in the literature emphasize the need for long-term postoperative surveillance (6,12).

The histopathological diagnosis of a mature teratoma is based on the identification of mature tissues derived from multiple germ layers (4). In the present case, H&E staining demonstrated mature epithelial, adipose, osseous and neural tissue components. Immunohistochemical findings provided additional evidence of multilineage differentiation. Pan-cytokeratin positivity supported epithelial differentiation, S100 positivity was compatible with neural or neuroectodermal differentiation and vimentin positivity supported mesenchymal differentiation (17). GFAP negativity provided additional evidence against a primary glial neoplasm, although this finding was not independently diagnostic (5). The Ki-67 proliferation index of ~5% was consistent with low proliferative activity (6). This pathological heterogeneity provides a basis for understanding the variable and typically non-specific CT and MRI findings of spinal teratomas. In the present case, CT revealed a mixed-density lesion within the spinal canal that contained band-like calcification; however, it did not demonstrate the other tissue components. This may have reflected the small proportion of fatty tissue and the limited soft-tissue contrast of CT. Despite CT being useful for identifying calcified or ossified components, MRI is required for further characterization as it can more adequately depict fatty, fibrous and cystic components (4,5).

On MRI, T2-weighted imaging demonstrated numerous small hyperintense cystic areas, suggesting fluid-containing cystic components within the tumor. Histopathologically, these areas may have corresponded to epithelial-lined cystic structures. Their relatively enclosed architecture may have restricted fluid mobility, contributing to high signal intensity on T2WI. By contrast, the band-like hypointense component on T2-weighted and fat-suppressed T2-weighted images was considered to correspond to the calcified component identified on CT and may have reflected mature bone or dense fibrous tissue. Water molecules are tightly bound within mineralized or collagenous matrices, shortening transverse relaxation (T2) times and thereby producing low signal intensity. Mineralized tissue may also produce local magnetic susceptibility effects, further accentuating the low-signal appearance on MRI. Mature bone and calcification may appear hyperdense on CT, whereas dense fibrous tissue may contribute to low signal intensity on MRI (4).

In the present case, the focal T1-hyperintense component demonstrated signal suppression on fat-suppressed T2-weighted images, suggesting the presence of fat within the tumor. Histopathologically, this finding was consistent with the mature adipose tissue identified within the lesion. Fat has a relatively short T1 relaxation time and therefore appears hyperintense on T1-weighted images, whereas fat-suppression techniques reduce the signal from fat protons, resulting in signal suppression (18). This imaging-pathology association has been reported in numerous studies regarding mature spinal cord teratomas and may thus provide a useful diagnostic clue for differentiating mature spinal teratomas from other intraspinal lesions (1,7). Contrast-enhanced T1-weighted imaging demonstrated heterogeneous enhancement of the solid components, with small non-enhancing areas. In conjunction with the H&E findings, the enhancing regions may have reflected vascularized soft-tissue components, including neural tissue, whereas the non-enhancing regions may have corresponded to cystic or fatty components (4,14). Septal or band-like enhancement may have reflected regional differences in vascularity and tissue composition, particularly the distribution of vascularized soft tissue, cystic components and fat. This enhancement profile reflected the tissue heterogeneity and compositional variation characteristic of mature spinal teratomas, providing useful diagnostic information.

The main diagnostic challenge in the present case was differentiation from other heterogeneous lesions in the conus medullaris region, including myxopapillary ependymoma, astrocytoma, cavernous malformation, dermoid cyst, epidermoid cyst and lipoma. Myxopapillary ependymoma was the leading preoperative consideration, given that the lesion was located in the conus medullaris and was associated with lower-limb radicular symptoms and heterogeneous enhancement on MRI. However, the combination of band-like calcification on CT, focal T1 hyperintensity with corresponding signal suppression on fat-suppressed T2-weighted images and multiple small T2-hyperintense cystic areas suggested the coexistence of calcified, fatty and cystic components, which was atypical for myxopapillary ependymoma. The absence of prominent hemorrhagic products, a hemosiderin cap sign or syringomyelia further reduced the likelihood of this diagnosis. In addition, the histopathological findings demonstrated mature tissue components derived from multiple germ layers, whereas GFAP negativity provided additional, although not definitive, evidence against an ependymal neoplasm or another primary glial neoplasm (5,8). Astrocytoma and cavernous malformation were considered less likely. Spinal astrocytomas typically cause infiltrative cord expansion and do not usually contain macroscopic fat or prominent calcification (5,19). Cavernous malformations may occasionally contain calcification; however, the absence of a compact ‘popcorn-like’ appearance, hemosiderin deposition or evidence of previous

hemorrhage, together with the presence of focal fat and cystic components, made this diagnosis less likely (20,21).

Dermoid cysts, epidermoid cysts and lipomas were also considered due to their overlapping fatty or cystic imaging features. Dermoid cysts typically contain fat, hair and sebaceous material, and typically demonstrate T1 hyperintensity, variable T2 signal intensity and little or no enhancement. However, calcification and heterogeneous enhancement may occasionally occur, resulting in notable imaging overlap with mature teratomas (22). Epidermoid cysts frequently demonstrate cerebrospinal fluid-like signal intensity with restricted diffusion and absent or thin peripheral enhancement (23). By contrast, intramedullary lipomas are characteristically fusiform, smoothly marginated lesions with homogeneous fat-equivalent signal intensity, marked signal suppression on fat-suppressed sequences and no notable enhancement (5,24). In the present case, the coexistence of band-like calcification, focal rather than homogeneous fat signal, multiple small cystic components and heterogeneous enhancement, together with mature tissues derived from multiple germ layers, favored the diagnosis of an IMMT.

Complete resection is the preferred treatment for spinal teratomas to relieve compression of the spinal cord and nerve roots, particularly for lesions located in the conus medullaris region (7,8). In the present case, gross total resection was achieved. At the last outpatient follow-up in October 2025, ~4 months after surgery, lower back pain and radiating pain had markedly improved, although mild residual numbness persisted in the left lower limb. This may be associated with the chronic neural injury caused by preoperative compression, as sensory recovery is generally slower compared with motor recovery. However, the follow-up period was relatively short and long-term postoperative imaging was not available. Therefore, long-term tumor control and the risk of recurrence could not be adequately assessed (6,12).

To conclude, spinal teratomas are rare spinal cord tumors, particularly in adults. When imaging findings are atypical or non-specific, clinical information should be integrated with histopathological and immunohistochemical findings to reduce the risk of missed or incorrect diagnoses. Histopathological examination remains key in definitive diagnosis and provides a basis for treatment planning, prognostic assessment and follow-up management.

Acknowledgements

Not applicable.

Funding

The present work was supported by the Natural Science Foundation of Guizhou Province [grant nos. Qiankehejichu-MS-(2026)-869 and Qiankehejichu-ZK-(2021)-yiban-479] and the Natural Science Foundation of Zunyi [grant no. Zunshike he-HZ-zi-(2025)-377].

Availability of data and materials

The data generated in the present study are included in the figures and/or tables of this article.

Authors' contributions

TR designed the present study and wrote the manuscript. LFS, XC, HZ and YYZ performed all the experiments. LYZ contributed to the histopathological examination and interpretation of the pathological findings. LJ contributed to the conception and design of the study. TR and LJ confirm the authenticity of all the raw data. All authors read and approved the final version of the manuscript.

Ethics approval and consent to participate

Not applicable.

Patient consent for publication

Written informed consent for publication was obtained from the present patient.

Competing interests

The authors declare that they have no competing interests.

References

1. Rahimizadeh A, Malekmohammadi Z, Samie S, Williamson WL and Amirzadeh M: Intramedullary mature teratoma with an exophytic component in an adult: Report of a case and literature review. Surg Neurol Int 11: 187, 2020.
2. Mohammadi A, Fereydouni T, Rahbari A, Mokarian P and Khademi Z: Intradural intramedullary teratoma presenting in the lumbar spine: Report of a rare case. World Neurosurg 106: 1051.e5-1051.e8, 2017.
3. Wang L, Li T, Gong M, Xing F, Li L, Xiao R and Guan Q: Intramedullary cervical spinal cord teratoma. Medicine (Baltimore) 99: e20107, 2020.
4. Zavala-Romero L, Villanueva-Castro E, Datta-Banik R, Ortiz-Altamirano AG, Rodriguez-Esquivel MM, Cienfuegos-Meza J and Arriada-Mendicoa JN: Mature teratoma at the lumbar spinal cord: A case report and literature review. Cureus 16: e52307, 2024.
5. Shih RY and Koeller KK: Intramedullary masses of the spinal cord: Radiologic-pathologic correlation. Radiographics 40: 1125-1145, 2020.
6. Kawai M, Nagoshi N, Iwanami A, Mikami S, Tsuji O, Fujita N, Yagi M, Watanabe K, Ishii K, Nakamura M and Matsumoto M.: Acute regrowth and dissemination of a mature spinal cord teratoma after partial resection. BMJ Case Rep 2018: bcr2017223742, 2018.
7. Saridakis N, Koumantzia C, Libard S, Marklund N and Eleftheriou A: Intramedullary holocord mature teratoma in an adult: A case report and review of the literature. Clin Neurol Neurosurg 195: 105925, 2020.
8. Turan N, Halani SH, Baum GR, Neill SG and Hadjipanayis CG: Adult intramedullary teratoma of the spinal cord: A case report and review of literature. World Neurosurg 87: 661.e23-661.e30, 2016.
9. Paterakis KN, Karantanas AH, Barbanis S, Hadjigeorgiou GM and Karavelis A: Cervical spinal cord intramedullary teratoma. Clin Neurol Neurosurg 108: 514-517, 2006.
10. Ciesla N, Dinglas V, Fan E, Kho M, Kuramoto J and Needha D: Manual muscle testing: A method of measuring extremity muscle strength applied to critically ill patients. J Vis Exp 12: 2632, 2011.
11. Yu J, Qu L, Li Y and Huang H: Coexistence of spinal teratoma of the conus medullaris and arteriovenous malformation in an adult: A case report. Turk Neurosurg 22: 510-514, 2012.
12. Nonomura Y, Miyamoto K, Wada E, Hosoe H, Nishimoto H, Ogura H and Shimizu K: Intramedullary teratoma of the spine: Report of two adult cases. Spinal Cord 40: 40-43, 2002.
13. Cunningham C, Flores C, Dabecco R, Nisarga P, Ahn J and Williamson R: Symptomatic mature teratoma of the lumbar spine: A case report. Surg Neurol Int 13: 16, 2022.

14. Arora S, Chumber S and Vani K: Intramedullary teratoma of spine in an adult patient. J Belg Soc Radiol 106: 84, 2022.
15. Eslami M, Ilaghi M, Shahabinejad E, Khajepour F, Karamouzian S and Reihani-Kermani H: Mature teratoma of conus medullaris: A case report and review of literature. Clin Case Rep 11: e7966, 2023.
16. Schmidt RF, Casey JP, Gandhe AR, Curtis MT and Heller JE: Teratoma of the spinal cord in an adult: Report of a rare case and review of the literature. J Clin Neurosci 36: 59-63, 2017.
17. Moon HJ, Shin BK, Kim JH, Kim JH, Kwon TH, Chung HS and Park YK: Adult cervical intramedullary teratoma: First reported immature case: Case report. J Neurosurg Spine 13: 283-287, 2010.
18. Gaeta M, Galletta K, Cavallaro M, Mormina E, Cannizzaro MT, Lanzafame LRM, D'Angelo T, Blandino A, Vinci SL and Granata F: T1 relaxation: Chemo-physical fundamentals of magnetic resonance imaging and clinical applications. Insights Imaging 15: 200, 2024.
19. She D, Lu Y, Xiong J, Geng D and Yin B: MR imaging features of spinal pilocytic astrocytoma. BMC Med Imaging 19: 5, 2019.
20. Jeon I, Jung WS, Suh SH, Chung TS, Cho YE and Ahn SJ: MR imaging features that distinguish spinal cavernous angioma from hemorrhagic ependymoma and serial MRI changes in cavernous angioma. J Neurooncol 130: 229-236, 2016.
21. Panda A, Diehn FE, Kim DK, Bydon M, Goyal A, Benson JC, Carr CM, Rinaldo L, Flemming KD and Lanzino G: Spinal cord cavernous malformations: MRI commonly shows adjacent intramedullary hemorrhage. J Neuroimaging 30: 690-696, 2020.
22. Juliansyah BP, Saito K, Takahashi Y, Anugerah SW, Nishizawa T, Ito A, Faried A, Sasaki T, Kanno H and Endo T: Challenges in diagnosing and treating lumbosacral dermoid cyst in an older patient: Illustrative case. J Neurosurg Case Lessons 11: CASE25883, 2026.
23. Dodson V, Majmundar N, Sharer LR and Gillick JL: Epidermoid cyst of the lumbar spine after lumbar puncture: A clinical, radiographic, and pathologic correlation. World Neurosurg 137: 363-366, 2020.
24. Dauleac C, Meyronet D, Ducray F, Mertens P and Cotton F: Magnetic resonance imaging features in intramedullary tumors: a pictorial review. Biomedicines 14: 1239, 2026.

Copyright © 2026 Ren et al. This work is licensed under a Creative Commons Attribution-NonCommercial-NoDerivatives 4.0 International (CC BY-NC-ND 4.0) License.